



Degradation of Lindane by persulfate/ferrioxalate/solar light process: Influential operating parameters, kinetic model and by-products

Leandro O. Conte^{a,b}, Giuseppe Legnettino^c, David Lorenzo^a, Salvador Cotillas^a, Marina Prisciandaro^c, Aurora Santos^{a,*}

^a Department of Chemical Engineering and Materials, Faculty of Chemical Sciences, Complutense University of Madrid, Avenida Complutense s/n, 28040 Madrid, Spain

^b Instituto de Desarrollo Tecnológico para la Industria Química (INTEC), Consejo Nacional de Investigaciones Científicas y Técnicas (CONICET) and Universidad Nacional del Litoral (UNL), Ruta Nacional N 168, 3000 Santa Fe, Argentina

^c Department of Industrial and Information Engineering and Economics, University of L'Aquila, Piazzale Ernesto Pontieri, Monteluco di Roio, 67100 L'Aquila, Italy

ARTICLE INFO

Keywords:

Lindane
Solar light
Modeling
Persulfate
Advanced oxidation process

ABSTRACT

This work describes the removal of lindane by persulfate activated with ferrioxalate under simulated solar light irradiation and circumneutral pH conditions. The influence of the main operating parameters is evaluated, and a kinetic model based on a radical mechanism is proposed and validated. To do this, synthetic solutions polluted with lindane and different amounts of oxidant and catalyst were employed. Results show that it is possible to completely remove lindane in 300 min using 2.29 mM persulfate and 0.12 mM ferrioxalate. Furthermore, chloride mineralization higher than 90% is achieved under these conditions. On the other hand, the main intermediate organic compounds are identified, and a degradation pathway based on the formation of sulfonated organics is proposed. Finally, the kinetic model proposed fits well with the experimental results and can help to predict the degradation of lindane in more complex effluents and under different operating conditions.

1. Introduction

Lindane is a pesticide manufactured and used in the 20th century worldwide. This organochlorine compound (γ -hexachlorocyclohexane, $C_6H_6Cl_6$) was synthesized using benzene and chlorine under UV irradiation [1]. The International Agency for Research on Cancer classified this pesticide as a cancerogenic compound, and the European Union forbade its production in 2008 [2]. However, there are still many illegal industrial landfills where chemical companies dumped tonnes of lindane and other isomers of HCH over the years, causing soil and groundwater pollution by leaching [3–5]. This is more problematic in the case of sites near rivers or reservoirs that supply water to the population because they may be susceptible to contamination by these organochlorine compounds, increasing the risk of fatal diseases. For this reason, it is necessary to develop clean and efficient technologies that allow the removal of lindane from water and groundwater.

Biological processes have been tested for the degradation of lindane since these technologies are low-cost and environmentally friendly [6–10]. Okeke et al. [9] studied the biodegradation of γ -HCH and α -HCH in water and soil slurry using two isolated *Pandoraea* sp. bacteria (LIN-1 and LIN-3),

achieving γ -HCH removal percentages of 25% and 45.5% with LIN-1 and LIN-3, respectively, in water within two weeks. Furthermore, this bacterium removed 150 mg L⁻¹ γ -HCH and α -HCH up to 89.9% and 93.3% in the liquid phase after eight weeks. More recently, Kumari et al. [7] evaluated artificial consortia of microalgae and bacteria to remove lindane in water. They degraded 50 mg L⁻¹ Lindane in 120 h, promoting the formation of intermediate metabolites such as pentachlorocyclohexenes, tetrachlorocyclohexenes, trichlorocyclohexane, dichlorocyclohexane, aliphatic chlorinated compounds and phenols. These biological technologies can remove lindane from aqueous matrixes but favor the generation of other organochlorine compounds that can also be toxic. In addition, the operation times required for the biodegradation of lindane are very long. The application of physicochemical processes to remove lindane from the water was also evaluated [11–14] to overcome these limitations. The use of amino-propyl silica gel-immobilized calix[6]arene was studied as an adsorbent for γ -HCH removal by Tor et al. [11]. The influence of pH, contact time, initial lindane concentration, calix[6]arene concentration, ionic strength and matrix composition was evaluated on lindane removal, finding that the maximum pesticide elimination was obtained at pH values within the range 2–8, and the sorption equilibrium was reached in 2 h. The higher the ionic strength, the higher the process efficiency. Specifically, total lindane

* Corresponding author.

E-mail address: aurasan@ucm.es (A. Santos).

<https://doi.org/10.1016/j.apcatb.2022.122288>

Received 25 September 2022; Received in revised form 9 December 2022; Accepted 11 December 2022

Available online 21 December 2022

0926-3373/© 2022 The Author(s). Published by Elsevier B.V. This is an open access article under the CC BY-NC-ND license (<http://creativecommons.org/licenses/by-nc-nd/4.0/>).

Nomenclature**Abbreviations**

AOPs	advanced oxidation processes
B#	blank runs
BDF	Backward Differentiation Formulae
CI	95% confidence interval of estimated parameters
Cl-PhOs	chlorinated phenolic compound
COCs	Chlorinated organic compounds
D#	non-irradiated runs
E#	irradiated runs
ECD	Electron Capture Detector
FID	Flame Ionization Detector
GC	Gas Chromatography
HCH	Hexachlorocyclohexane
High-Rad	solar radiation fluxes found in Madrid city measured in September (beginning), during the period of the maximum incident light on clear days, with standard relative humidity conditions (40–60%)
ISTDs	internal standards
Low-Rad	solar radiation fluxes found in Madrid city measured in January (mid), during the period of the maximum incident light on clear days, with standard relative humidity conditions (40–60%)
LVRPA	local volumetric rate of photon absorption
Mid-rad	solar radiation fluxes found in Madrid city measured in November (end) during the period of the maximum incident light on clear days, with standard relative humidity conditions (40–60%)
MSD	Mass Spectrometric Detector
PCXEs	pentachlorocyclohexene isomers
PS	persulfate
RP	Reaction path
SM	Supplementary material
SPME	solid phase microextraction
SQR	sum of quadratic squares
TCBs	trichlorobenzene isomers
TCXEs	tetrachlorocyclohexene isomers

Symbols

$\langle e^a(z, t) \rangle_{V_{irr}}$	The volumetric average of the LVRPA in the irradiated reactor volume, $EL^{-1} \min^{-1}$
C_j	concentration of compound j, mM
$e^a(z, t)$	The average value of the LVRPA axial reactor coordinate z, $EL^{-1} \min^{-1}$
$e^a(z, t, \lambda)$	local volumetric rate of photon absorption at each reactor position (z), time (t) and wavelength (λ), $E L^{-1} \min^{-1}$
K_{eq}	equilibrium constant to form the complex $Fe^{3+}(C_2O_4)_3^{3-}$,

$$K_{eq} = 5 \cdot 10^{10} \text{ mM}^{-3}$$

k_i	kinetic constant of reaction i, units depending on the reaction order, time in min and concentration in mM
L_{irr}	the length of the irradiated reactor, cm
$P(1 - 5)$	chlorinated by-products (P_1 to P_5) generated in the dechlorination reactions
q_w	discretized spectral radiation flux incident at the reactor window for each wavelength, $E_{min}^{-1} \text{ cm}^{-2}$
r_i	reaction rate, $\text{mM} \cdot \text{min}^{-1}$ related to the total volume of the batch system
R_j	Production rate of compound j in $\text{mM} \cdot \text{min}^{-1}$
t	time, min
T	temperature
V	volume, L
V_{irr}	irradiated reactor volume, L
x	The number of sulfate radicals involve in dechlorination reactions
X_j	conversion of compound j
z	axial reactor coordinate, cm

Greek Letters

α_λ	molar absorptivity of ferrioxalate, $\text{mM}^{-1} \text{ cm}^{-1}$
ϕ_G	global quantum yield, $\text{mmol} \cdot \text{E}^{-1}$
κ_λ^T	volumetric absorption coefficient of the medium, cm^{-1}
κ_λ	volumetric absorption coefficient at each wavelength of the specie absorbing light, cm^{-1}
λ	Wavelength, nm
ν_{ij}	is the stoichiometric coefficient of the compound j in reaction i (<0 for reactant and >0 for products)
ν_T	species-reactions matrix

Subscripts

calc	calculated
Cl	dechlorination
exp	experimental
irr	irradiated
L	lindane
max	maximum
min	minimum
o	initial
ox – m	oxalate experimentally measured corresponds to the sum of free oxalate anions and oxalate in the ferrioxalate complex
PS	persulfate
t	total
w	window

removal was obtained using an ionic strength higher than 3% wt. because adding salts can decrease Lindane's solubility and increase its sorption. Liquid-liquid extraction has also been evaluated for removing lindane [12]. Due to its high stability and distribution coefficient, high separation efficiencies were attained with the solvent petro-ether-chloroform. Physico-chemical processes allow the efficient removal of the target pollutant in short operation times but do not degrade it, only separate it. Therefore, a subsequent step is required to eliminate lindane from the adsorbents or solvents used in these technologies.

Advanced Oxidation Processes (AOPs) can be considered an efficient and environmentally friendly alternative to biological and physico-chemical processes for degrading organic pollutants in water bodies [13]. These processes are based on producing large amounts of free radicals (hydroxyl, sulfate, carbonate...) that can attack the pollutants,

favouring their degradation and even their complete chlorine mineralization. Different AOPs have been evaluated for the degradation of lindane in water [14–20]. Nitoi et al. [14] studied the photo-Fenton mechanism and kinetics of 3.47 μM lindane degradation in water using high concentrations of iron and hydrogen peroxide (3.67 mM in Fe^{2+} and about 29.41 mM H_2O_2) and UV light. They concluded that the degradation rate followed a pseudo-first-order kinetic model concerning lindane and chlorine mineralization, reaching a chlorine mineralization efficiency of 95% within 1 h. The application of the UV-C/persulfate system for removing lindane in water (3.43–17 μM) was reported by Khan et al. [20]. A synergistic effect of H_2O_2 (0.1 mM) and $S_2O_8^{2-}$ (0.1 mM) was found in this work, confirming that the formation of sulfate radicals in the solution promoted pesticide degradation. Degradation and mineralization of lindane depended on the UV fluence. Khan

et al. [15] studied the lindane ($3.43\mu\text{M}$) oxidation with PMS ($0.125\text{--}1\text{ mM}$) and UV light (254 nm) with a lindane conversion higher than 90% in 3 h. Dominguez et al. [18] evaluated the treatment of groundwater polluted with organochlorine pesticides from lindane production wastes by electrochemical oxidation with diamond electrodes. The elimination of four isomers of HCH (including Lindane) was reached in 4 h by applying a current intensity of 0.4 A. Furthermore, this technology could mineralize all the organic matter contained in the groundwater by up to 90%. These authors treated also a synthetic aqueous solution of lindane ($17.18\text{--}3.43\mu\text{M}$) by electrochemical oxidation with diamond electrodes [16] with similar results. A photocatalytic removal of 99% of lindane in the aqueous solution ($1\mu\text{M}$) was achieved at 360 min [19] with a solar light-activated TiO_2 (SSLA- TiO_2) using a 300 W Xenon lamp and simultaneous addition of persulfate and hydrogen peroxide (0.1 mM each). More details of these works can be found in Table SM-1 of the supplementary Information. As shown in Table SM-1, most of the kinetic models proposed are empirical models considering first-order reactions for lindane degradation. Only the work of Nitoi et al. [14] propose a kinetic model based on a mechanism for lindane degradation with $\text{UV}/\text{H}_2\text{O}_2/\text{Fe}$ at pH 3. Khan et al. [15] proposed a competitive mechanism to determine the kinetic constant between lindane and sulfate radicals. Lindane oxidation with Persulfate/ H_2O_2 has been studied by Khan et al. [20] using UV light. These authors proposed a first-order kinetic model for lindane that does not quantitatively include the effect of other variables in the kinetic model. Neither a kinetic model is proposed to explain chloride mineralization.

AOPs have demonstrated a high ability to remove lindane from water. However, the specific experimental conditions (acidic conditions) and the energy costs required for developing these processes may compromise their large-scale application. Direct sunlight irradiation could drastically reduce the energy costs associated with UV lamps. Likewise, using iron sources (iron complexes) that allow working under circumneutral pH conditions could avoid the need for a subsequent neutralization step before discharge into the environment [21]. On the other hand, modeling of AOPs is a very useful tool for predicting process efficiency and reactor design. Mathematical models for different AOPs applied to a wide variety of pollutants have been reported in the literature [22–26]. This allows a more efficient optimization of process operating conditions.

With this background, the main aim of the present work is to evaluate the degradation of lindane in the aqueous phase using sunlight-activated persulfate in the presence of ferrioxalate as the catalyst. Persulfate has been used as an oxidant as sulfate radicals have been revealed to be more reactive against HCH than hydroxyl radicals [27]. A kinetic model to describe the removal of this pesticide and chlorine mineralization has been developed and discriminated by the applied technology. The influence of the main operating parameters on lindane removal and chlorine mineralization was experimentally studied and quantified with the kinetic model proposed. The main intermediate chlorinated by-products formed during the treatment of lindane polluted water were identified, and a dichlorination mechanism was proposed. From our knowledge, this work is the first to study lindane degradation using (simulated) solar light at circumneutral pH with persulfate as the oxidant. The kinetic model developed will be based on a radical mechanism. The kinetic model developed for lindane degradation and chloride mineralization will be based on a radical mechanism. This kinetic model should quantitatively explain the influence of the variables considered (persulfate, Lindane, ferrioxalate concentrations and irradiation), overcoming the limitations of empirical kinetic models commonly found in the literature. Hence, the process reported in this work opens the possibility of applying AOPs using solar light under mild operating conditions to eliminate lindane in aqueous phases.

2. Material and methods

2.1. Chemicals

Lindane was purchased from Merck. Ferrioxalate complex was prepared from potassium oxalate monohydrate (99.5%) and iron (III) sulfate x-hydrate ($\text{Fe}_2(\text{SO}_4)_3 \cdot x\text{H}_2\text{O}$, $x < 3\%$, Sigma Aldrich, Spain). Hexachlorobenzene and butyl cyclohexane (Sigma Aldrich, Spain) were used as standard internal compounds to quantify Chlorinated Organic Compounds (COCs). Scharlau, Spain, provided N-hexane for the extraction of Chlorinated Organic Compounds. Sodium thiosulfate was used for persulfate (PS) determination. In ionic chromatography, sodium carbonate, sodium bicarbonate, acetone, and oxalic acid were used for chloride measurement. 1,10-phenanthroline, and sodium acetate were used for the determination of iron. Sodium hydroxide or sulfuric acid employed for pH adjustment were purchased by Sigma Aldrich (Spain). All the stock solutions were prepared with high-purity water from a Millipore Direct-Q system (resistivity $>18\text{ M}\Omega\text{ cm}$ at 25°C).

2.2. Experimental set-up and procedure

The experimental runs were carried out in a cylindrical borosilicate glass flat-plate reactor (380 mL, 10 cm length) with external recycling. The reactor window (7 cm in diameter) is quartz to ensure good transmittance of incident radiation in the range of wavelengths of interest (UV-Vis). A solar simulator (Oriel, model 67005) was used as a radiation source. The experimental setup is schematized in Fig. 1. A detail of the reactor and the solar simulator is provided in Fig. S1 in the Supplementary Information. The storage tank includes a pH meter, a thermometer, a mixer, and a liquid sample valve. A circulating-thermostatic bath was used to ensure constant temperature during the reaction (PolyScience temperature controller). A liquid pump (NF 300 KT, Liqueiprot) was used to achieve a high recirculation rate (3 L min^{-1}) of the reactive solution between the storage tank and the photo-reactor, ensuring good mixing conditions of liquid in the reactor and the storage tank. The total volume of the treated solution was 2.0 L, while the irradiated reactor volume was 0.38 L.

Different configurations of the solar simulator system were analyzed to evaluate the influence of radiation on the process. Two working powers (210–240 W), an air mass filter (AM 1.5 G, ASTM E 892 standard, Newport Corp.), a liquid attenuation filter (Water Optical Filter, 1.5 Inch Series, Newport Corp.) and different distances from the radiation source to the reactor window (10 and 15 cm) were applied. From these configurations, it is possible to simulate solar radiation fluxes found in Madrid city, Spain. ($40^\circ30'\text{ N}$, $3^\circ40'\text{ E}$, 667 m above sea level) measured in September (beginning), November (end) and January (mid), during the period of the maximum incident light on clear days, with standard relative humidity conditions (40–60%). These conditions are named as High-Rad, Mid-rad and Low-Rad, respectively. Radiation fluxes were measured with a Flame UV-VIS spectrometer (Ocean Insight) coupled with a monocolin UV-Visible optical fiber ($\lambda_{\text{min}} = 300\text{ nm}$ and $\lambda_{\text{max}} = 550\text{ nm}$).

Local radiation fluxes averaged over the reactor window (q_w) simulating the solar conditions above cited in Madrid were $q_w = 4.61 \times 10^{-8}\text{ Ecm}^{-2}\text{s}^{-1}$ for Low-Rad, $q_w = 8.73 \times 10^{-8}\text{ Ecm}^{-2}\text{s}^{-1}$ for Mid-Rad, and $q_w = 1.12 \times 10^{-7}\text{ Ecm}^{-2}\text{s}^{-1}$ for High-Rad. These fluxes were obtained modifying the power, and the distance from the lamp to the reactor window.

Milli-Q water was saturated in lindane and then diluted with milli-Q water if necessary to achieve the desired lindane concentration in the aqueous phase. Water saturation in lindane was carried out under controlled temperature ($20 \pm 1^\circ\text{C}$) and 24 h of agitation; the γ -HCH saturation concentration achieved was 0.032 mM (9.31 mg L^{-1}). The concentrate ferrioxalate solution (oxalate/iron molar ratio of 10:1) was prepared according to the methodology described by Murov et al. [28].

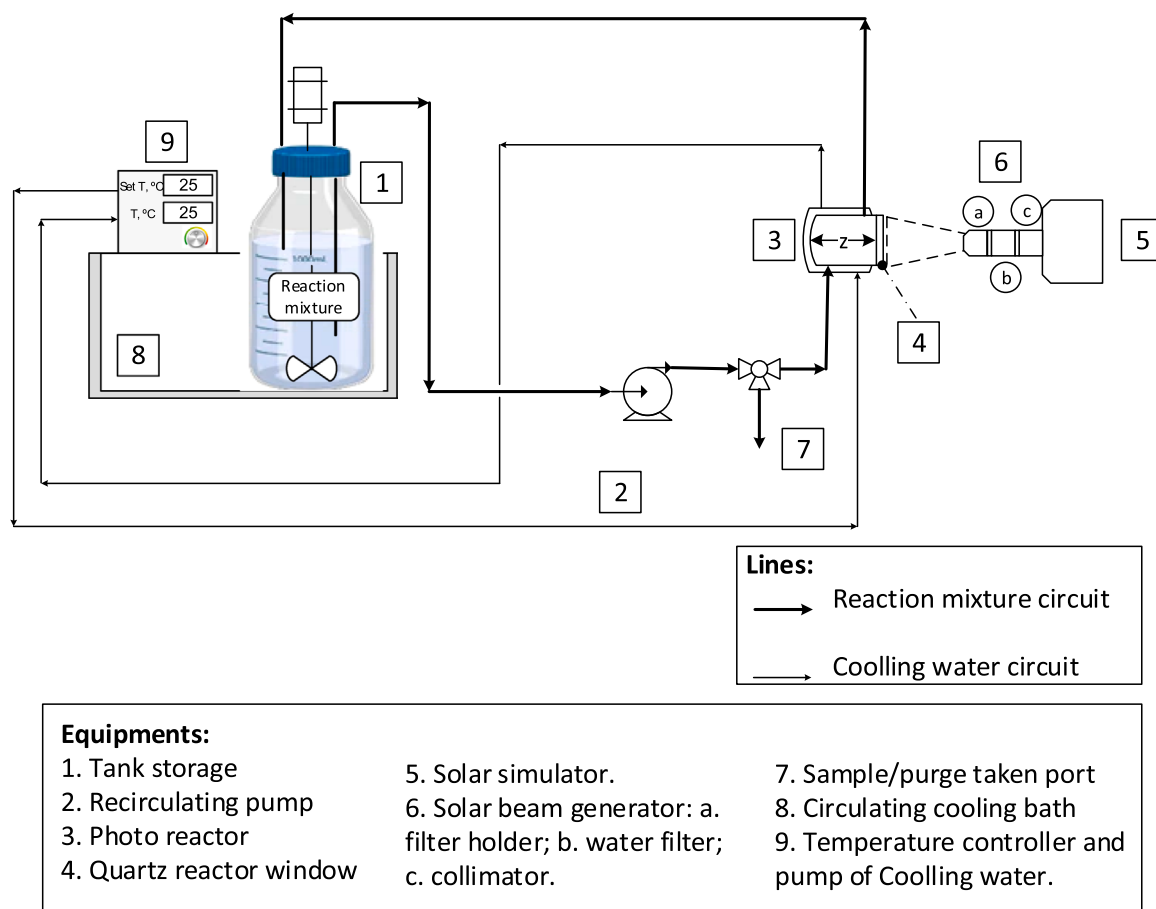


Fig. 1. Scheme of the experimental set-up.

The temperature (T) of the thermostatic bath was set to the desired temperature. A volume of 1.8 L of the lindane aqueous solution was placed in the storage tank, and 200 mL of the concentrated ferrioxalate solution was added to reach the desired Fe concentration in the final 2 L volume in the storage tank. The initial pH was close to neutrality (6.5–7). Recirculation was started by switching the liquid pump at a flow rate of 3 L min^{-1} , and a sample from the storage tank was taken (time 0). At zero time, the required volume of a concentrate PS solution (400 mM) was added to the storage tank to reach the desired oxidant concentration. The lamp shutter was removed to start the irradiation experiments.

Aqueous samples were taken from the storage tank at different times during the reaction. After that, sodium thiosulfate was used to stop the reaction, reducing the remaining persulfate in the samples. The time interval studied ranged from 0 to 6 h. lindane and organic oxidation by-products, remaining PS, oxalate, and pH were determined in the aqueous phase at different times. The sample preparation is detailed in the text SM-1. The composition of the aqueous phase in the reactor and the storage tank was assumed to be the same due to the high recirculation flow rate; this assumption was experimentally validated. A set of

blank runs summarized in Table 1 were carried out to check: the lindane adsorption in the system (B1), the effect of irradiation (B2), the effect of PS and temperature (B3), the effect of PS and irradiation (B4) on lindane conversion.

The second set of runs was carried out to study the effect of the operation conditions. lindane concentration range ($0.030 - 0.006 \text{ mM}$) has been chosen, taking into account the concentration of the HCH isomers experimentally found in groundwaters near the lindane production sites. As an example, HCHs concentration in the most contaminated areas of Sardas and Bailin Landfills (Sabiñanigo, Spain) where HCH values up to 0.051 mM are reported [5,29,30]. Irradiation used ($q_w = 0.0; 4.61 \cdot 10^{-8}; 8.73 \cdot 10^{-8}$ and $1.1210^{-7} \text{ E cm}^{-2} \text{ s}^{-1}$) simulated three solar radiation fluxes found in Madrid city, Spain; and iron concentration ($0.06 - 0.17 \text{ mM}$). The pH of the experiment was natural. The experimental conditions of the runs are summarized in Table 2. PS concentration ($2.29 - 8.69 \text{ mM}$) was selected considering the limitations for sulfate anion in water discharges and the theoretical stoichiometric amount of sulfate radicals required for lindane mineralization (Eq. (1)). In the activation of PS by iron 1 mol of PS produces 1 mol of sulfate

Table 1
Experimental conditions of blank runs.

Run	C_{PS_0} (mM)	C_{Ox_0} (mM)	$C_{Fe^{3+}}$ (mM)	C_{L_0} (mM)	T (°C)	$q_w \cdot 10^7 (\text{E cm}^{-2} \text{ s}^{-1})$	Stoichiometric Ratio ^a
B1	0.00	0	0	0.032	25	Dark	0
B2	0.00	0	0	0.032	25	1.12	0
B3	8.69	0	0	0.032	35	Dark	11.32
B4	2.29	0	0	0.032	25	1.12	2.98

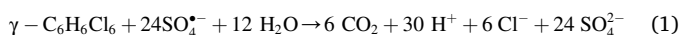
^a $tq \text{ ratio} = \left(\frac{C_{PS_0}}{C_{L_0}} \right) / 24$ is calculated as the molar ratio of PS to L divided by 24, according to Eq. (1).

Table 2Experimental conditions of the runs. pH₀ = 6.7.

Run	C _{PS₀} (mM)	C _{OX₀} (mM)	C _{Fe³⁺} (mM)	C _{L₀} (mM)	T (°C)	q _w · 10 ⁷ (E cm ⁻² s ⁻¹)	Stoichiometric Ratio ^a
D1	8.69	1.70	0.17	0.015	35	0.00	24.14
D2	3.25	1.20	0.12	0.015	35	0.00	9.03
D3	3.25	1.20	0.12	0.030	25	0.00	4.51
E1	3.25	1.20	0.12	0.021	25	1.12	6.45
E2	3.25	1.20	0.12	0.021	25	0.46	6.45
E3	3.25	1.20	0.12	0.006	25	0.87	22.57
E4	3.25	1.20	0.12	0.006	15	0.87	22.57
E5	3.25	0.60	0.06	0.030	25	1.12	4.51
E6	8.69	1.70	0.17	0.015	25	1.12	24.14
E7	2.29	1.40	0.14	0.010	25	1.12	9.54
E8	2.29	1.20	0.12	0.030	35	1.12	3.18
E9	3.25	1.40	0.14	0.006	35	1.12	22.57

^a tq ratio = $\left(\frac{C_{PS_0}}{C_{L_0}}\right)/24$ is calculated as the molar ratio of PS to L divided by 24, according to Eq. (1)

radicals. The ratio of PS to the stoichiometric amount required to mineralize the initial lindane in the aqueous phase is also indicated in Table 1. An excess of PS was always used to ensure enough oxidant remains in the reaction media despite the oxidant consumption by non-productive reactions.



2.3. Analytical methods

The concentration of lindane and other COCs present in the system were quantified by Gas Chromatography (GC) with a Flame Ionization Detector (GC/FID) and an Electron Capture Detector (GC/ECD), simultaneously. Previously, the aqueous phase (4 mL) was extracted with n-hexane (0.8 mL). The mixture of both phases was shaken, followed by 10 min of settlement, allowing the organic phase separation by decantation. For the GC/FID/ECD assays performed, a chromatography column HP-5MS was used as a stationary phase, and a constant flow rate of helium was used as a mobile phase (1.7 mL min⁻¹). The chromatographic oven worked under a programmed temperature gradient. Butyl cyclohexane and Hexachlorobenzene were added to the organic samples as internal standards (ISTDs) for FID and ECD analyses. Under these analytical conditions, the detection limits were 0.035–0.35 μM, which referred to the organic concentration in the water before the extraction with n-hexane. Further details of the analytical methods used have been reported elsewhere [29,31]. The PS concentration was determined by a colorimetric method, using a BOECO S-20 UV–VIS spectrophotometer at 352 nm within the detection limits of 0–50 mM [32]. Total iron concentration was determined by colorimetric titration, using a spectrophotometer (BOECO S-20 UV–VIS, Germany) at 510 nm [21] and concentrations calibrated in the range of 0–0.2 mM [33]. The pH was measured with a Basic 20-CRISON (Barcelona, Spain) electrode. Additionally, organic acids by-products and chlorides were measured by Ion Chromatography (Metrohm, Swiss) with anionic chemical suppression and a conductivity detector, using a SUPP5 5–250 column (25 cm length, 4 mm diameter) and solution of Na₂CO₃ (3.2 mM) and NaHCO₃ (1 mM) as mobile phase (0.7 mL min⁻¹).

The reaction byproducts were identified and quantified using an HP6890 Gas Chromatograph and an HP5973 Mass Spectrometric Detector (MSD) coupled with a CTC CombyPAL (GC sampler 80). The organic species were extracted from the liquid phase by solid phase microextraction (SPME). 10 mL of reaction sample were put in contact with a Polyacrylate (PA) coating fiber (3600 s at 50 °C) in a 10 mL glass-vial without headspace. In splitless mode, the desorption was conducted in the injector at 270 °C (180 s).

3. Results and discussion

Lindane (γ-HCH) conversion was calculated by Eq. (2).

$$X_L = \frac{C_{L_0} - C_L}{C_{L_0}} \quad (2)$$

Being C_{L₀} and C_L the lindane concentration at zero time and at reaction time, respectively.

Dechlorination (chlorine mineralization) achieved was calculated by Eq. (3).

$$X_{Cl} = \frac{C_{Cl^-}}{6 C_{L_0}} \quad (3)$$

being C_{Cl⁻} and (6 C_{L₀}) the chloride concentration released up a time, and the initial chloride in the lindane concentration at zero time, respectively. Dechlorination degree lower than lindane conversion implies that chlorinated organic compounds remain in the reaction media.

The total oxalate (sum of oxalate as free anion or complexed with iron) conversion is calculated according to Eq. (4).

$$X_{ox-m} = \frac{C_{ox-m o} - C_{ox-m}}{C_{ox-m o}} \quad (4)$$

Being C_{ox-m o} and C_{ox-m} the total oxalate concentration at zero time and at a reaction time, respectively.

The oxidant conversion is calculated by Eq. (5).

$$X_{PS} = \frac{C_{PS_0} - C_{PS}}{C_{PS_0}} \quad (5)$$

Being C_{PS₀} and C_{PS} the oxidant (PS) concentration at zero time and at a reaction time, respectively.

lindane conversion in blank runs B1 to B4 (not shown) was lower than 10% in 6 h. In addition, dechlorination measured was negligible in these runs.

The following subsections show and discuss the effect of irradiance, temperature, iron concentration, oxidant concentration and lindane concentration on the lindane conversion, dechlorination degree, oxalate conversion and oxidant consumption. The pH was kept at neutral conditions for all the runs during the whole reaction time.

3.1. Effect of irradiance

The experimental section explains that dark runs and three irradiance levels have been used. Fig. 2 shows the profiles with time obtained in non-radiated runs (D1, D2, D3). lindane conversion, dechlorination degree, oxalate conversion and PS conversion are shown in Fig. 2a, b, c and d, respectively.

A positive effect of temperature (D2 vs D3) and a small effect of the oxidant concentration (D1 vs D2) on the lindane conversion were

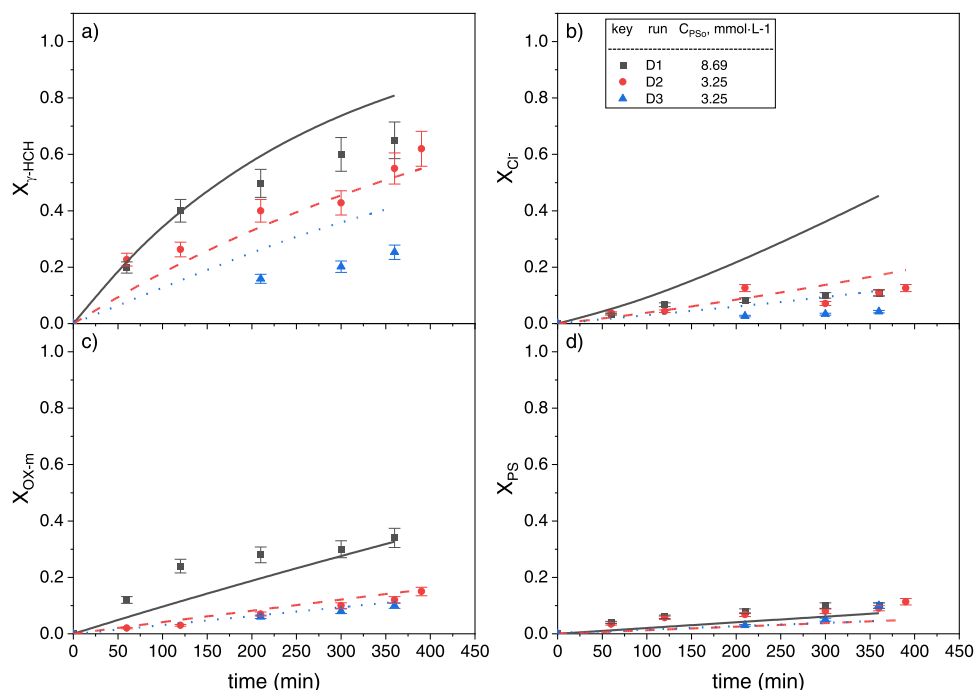


Fig. 2. Lindane conversion (a), dechlorination degree (b), oxalate conversion (c) and oxidant conversion (d) in non-irradiated runs D1, D2 and D3 in Table 1. Symbols depicted experimental values. Lines show predicted values with Eqs. (23)–(34).

noticed in the dark runs. lindane conversion obtained at 6 h in run D1 ($T = 35^\circ\text{C}$) was about 0.7 at 6 h reaction time. Dechlorination achieved under dark conditions was much lower than lindane conversion, suggesting the presence of chlorinated by-products in the reaction media. Low oxalate and oxidant conversion were noticed in the absence of light.

The effect of irradiation under the same initial conditions for the other variables considered is shown in Fig. 3 (runs E1 and E2 in Table 2). Small differences between lindane (a) and oxidant conversion (d) at the highest and lower irradiation are found. On the contrary, dechlorination

(b) and oxalate conversion achieved at the lowest radiation are lower than obtained at the highest irradiation conditions.

The dechlorination degree in runs E1 and E2 is lower than lindane conversion at the initial stages, indicating the presence of chlorinated by-products. However, almost total dechlorination and lindane conversion are reached at the final time studied. These results imply that chlorinated organic compounds are removed from the reaction media at this reaction time. Moreover, complete lindane removal and dechlorination were achieved at 3 h at the higher irradiation level (E1). As

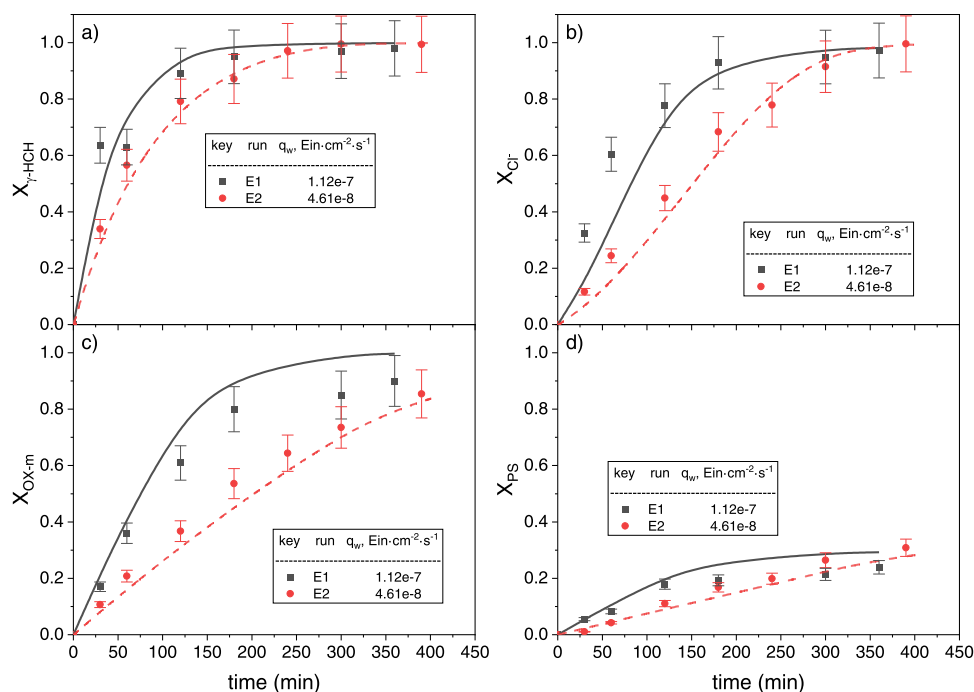


Fig. 3. Effect of radiation on lindane conversion (a), dechlorination degree (b), oxalate conversion (c) and oxidant conversion (d) (runs E1 and E2 in Table 2). Symbols depicted experimental values. Lines show predicted values with Eqs. (23)–(34).

shown in Fig. 3, when the oxalate achieves high conversion, the oxidant conversion reaches an asymptote (Fig. 3c, d). This is explained by the ferrioxalate complex disappearance, stopping the radical oxidant production. The work of Nitoi et al. [14] uses an irradiance value of $6 \cdot 10^{-6} \text{ Es}^{-1}$ with UV light applied to eliminate lindane with $\text{UV}/\text{H}_2\text{O}_2/\text{Fe}$ (the reactor volume or dimensions are not provided). The irradiance used in the present work ranges from $1.74 \cdot 10^{-7} \text{ Es}^{-1}$ to $4.25 \cdot 10^{-7} \text{ Es}^{-1}$. He et al. [34] used $2.5 \cdot 10^{-6} \text{ Es}^{-1} \text{ L}^{-1}$, with an optical path of 1.42 cm and irradiated volume of 0.050 L and UV light. The irradiances used in this work (reactor volume 0.38 L, optical path 10 cm) are $4.57 \cdot 10^{-7}$ and $1.11 \cdot 10^{-6} \text{ Es}^{-1} \text{ L}^{-1}$. Therefore, the good results obtained with simulated solar light at similar conditions of irradiance values than those used with UV reactors encourage the use of solar light in the abatement of highly chlorinated pesticides such as Lindane.

3.2. Effect of temperature

The temperature effect on the composition of the reaction media was examined at the highest radiation used tested, in the range 15–25°C, using similar initial conditions of the other variables (runs E4 and E3 in Table 1). Results are shown in Fig. 4. Small differences are found in lindane (a), oxalate (c) and oxidant conversion (d) at the highest and lower temperatures used. Lindane conversion achieved was higher than 95% at 6 h. Again, dechlorination was lower than lindane conversion at the initial stages, suggesting that chlorinated byproducts appear and accumulate in the media at this stage. However, similar dechlorination degrees and lindane conversion (higher than 90%) are obtained at 6 h at both temperatures.

3.3. Effect of iron concentration

The effect of initial iron (III) on the evolution of the reaction media was tested at the highest radiation used, using similar conditions for the rest of the variables studied.

The influence of iron concentration at the highest radiation is shown in Fig. 5 (runs E1 and E5 in Table 2). Small differences in lindane and oxalate conversion were found at both catalyst concentrations (0.06 and

0.12 mM), the differences within the experimental error. On the contrary, a remarkable effect of the iron concentration was found on dechlorination degree. The lower the catalyst concentration, the lower the dechlorination achieved. However, even at the lower iron concentration, a high lindane conversion and significant dechlorination are obtained at 6 h of irradiation (80%). PS conversion was lower than 25% in both runs. High lindane conversion and dechlorination have been obtained at neutral pH using low catalyst concentrations (ferrioxalate complex). This avoids the high catalyst concentration and acidic pH required using Fe^{2+} as a catalyst and UV-C light [14]. Moreover, the photoactivation of the catalyst by solar light is more convenient than UV lamps with high energy cost.

3.4. Effect of oxidant concentration

The effect of persulfate on the evolution of the reaction media was tested at the highest radiation used, at 25 °C and under similar conditions for the other variables studied. Results are presented in Fig. 6 (runs E6, E7 in Table 2). As shown, the lower the oxidant concentration, the lower the lindane conversion (a), dechlorination achieved (b) and oxalate conversion (c). Again, the main differences between lindane conversion and dichlorination degree are noticed at the initial stages. However, similar lindane conversion (higher than 95%) and dechlorination degrees (higher than 90%) were obtained at 6 h of reaction at both oxidant concentrations used (2.29 and 8.69 mM). It should be noticed that the differences in dechlorination, lindane and oxalate conversion profiles in runs E6 and E7 are relatively low, considering the high difference in the oxidant concentration used in these runs. This fact can be attributed to unproductive reactions, as explained in the following section. As expected, the PS conversion decreases as the oxidant concentration increases due to excess oxidant use (Fig. 6d).

3.5. Effect of lindane concentration

The effect of lindane concentration on the evolution of the reaction media was tested at the highest radiation used, at 35°C and under similar conditions of the other variables studied. Results are shown in Fig. 7 (runs E8, E9 in Table 2). Slighter lower lindane conversion is noticed at

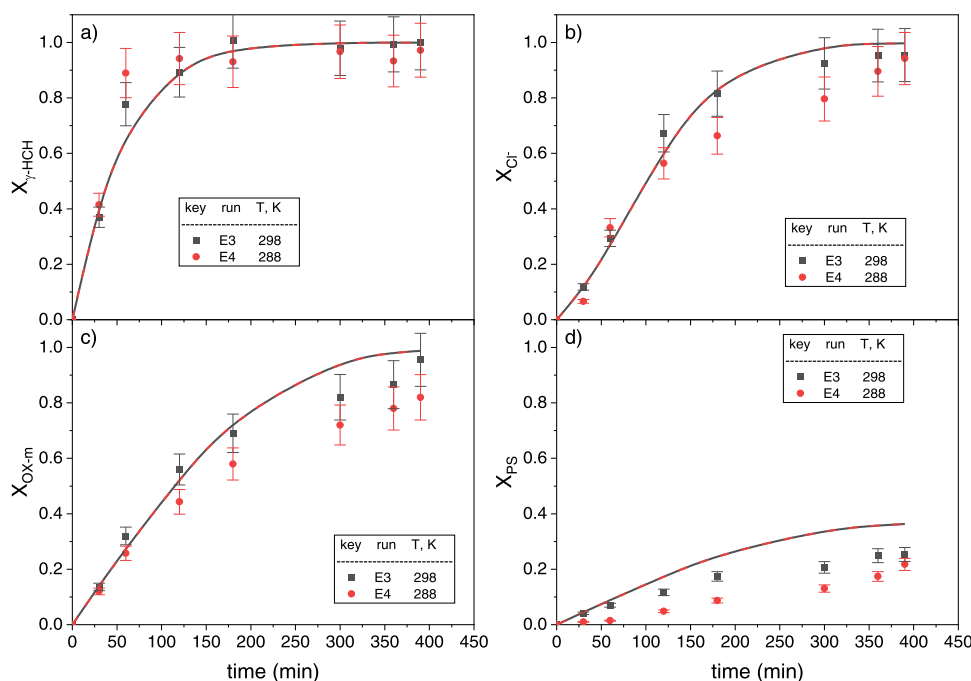


Fig. 4. Effect of temperature on lindane conversion (a), dechlorination degree (b), oxalate conversion (c) and oxidant conversion (d) (runs E3 and E4 in Table 2). Symbols depicted experimental values. Lines show predicted values with Eqs. (23)–(34).

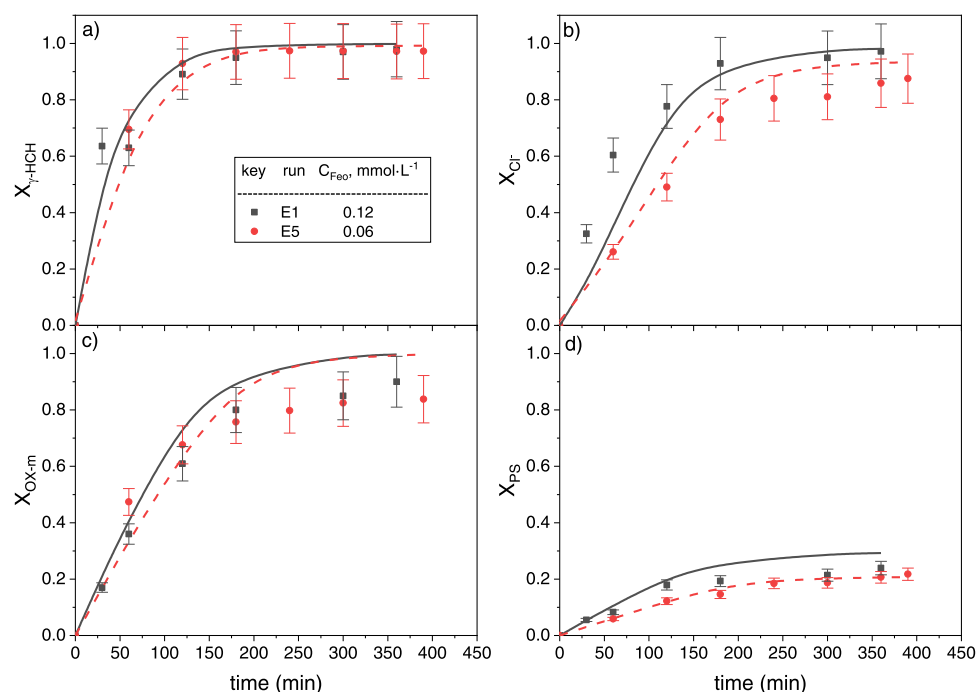


Fig. 5. Effect of iron concentration on lindane conversion (a), dechlorination degree (b), oxalate conversion (c) and oxidant conversion (d) (runs E1 and E5 in Table 2). Symbols depicted experimental values. Lines show predicted values with Eqs. (23)–(34).

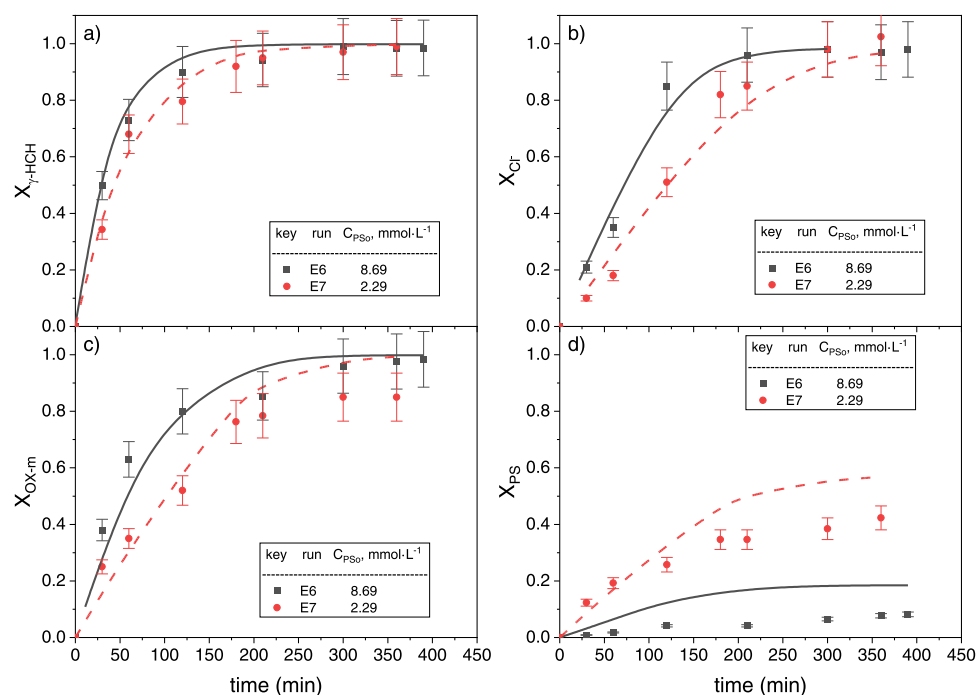


Fig. 6. Influence of oxidant concentration on lindane conversion (a), dechlorination degree (b), oxalate conversion (c) and oxidant conversion (d) (runs E6 and E7 in Table 2). Symbols depicted experimental values. Lines show predicted values with Eqs. (23)–(34).

the highest lindane concentration used. Dechlorination at 0.006 mM of lindane does not follow the same trend. The high experimental error in chloride measurement at the lowest lindane concentration can explain the anomalous values observed in run E9. Small differences were found in oxalate and PS conversion in both runs.

3.6. Chlorinated by-products

The reaction intermediates were identified and quantified by coupling GC-MSD and SPME. The analysed reaction samples were obtained under the condition of run E5. After 60 min of reaction, the conversion of lindane was 0.70, and the dechlorination degree achieved was 0.25. The identified products are summarized in Table 3. These compounds were identified using the NIST library (version NIST011)

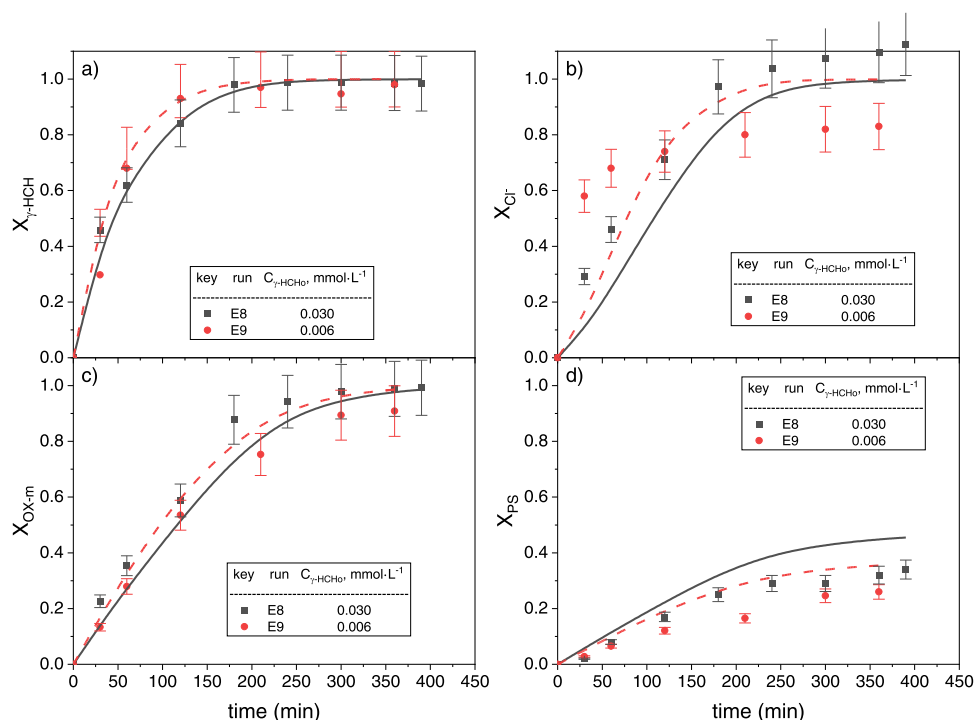


Fig. 7. Influence of initial lindane concentration on lindane conversion (a), dechlorination degree (b), oxalate conversion (c) and oxidant conversion (d) (runs E8 and E9 in Table 2) Symbols depicted experimental values. Lines show predicted values with Eqs. (23)–(34).

and the retention index obtained elsewhere [1]. The retention time (RT) and the concentration obtained for the identified by-products are summarized in Table 3.

Furthermore, no other peaks than those corresponding to compounds in Table 3 appear in the chromatogram. As can be seen, the chlorinated by-products identified are only 6% of the reacted lindane at 60 min in run E5 (70%). The dechlorination achieved at this time was 25% (Fig. 5). Therefore, about 39% of the chlorinated by-products remain unidentified at 60 min in E5. These unknown by-products could not be detected and identified using either GC/MSD or HPLC/DAD. Therefore, the formation of chlorinated by-products from lindane oxidation that cannot be detected by GC/MS or HPLC analysis must be considered. Ren et al. proposed a radical mechanism of sulfate radical capable of producing sulfonate compounds [35]. These compounds are generated by the direct attack of sulfate radical over the double bond. Formation of sulfonate compounds were also proposed by Pan et al. using persulfate as oxidant [36]. In this case, the double bond can be formed after sulfate radical first loss of chloride in the lindane oxidation.

The mechanism proposed is summarized in Fig. 8. Firstly, the sulfate anion radical promoted the abstraction of a hydrogen atom from the HCH ring producing the bisulfite radical and a carbanion. The latter compound promoted the releasing of the Cl^- as the living group and formed a double bond inside the HCH ring, producing the isomers of pentachlorocyclohexene (PCXEs). It was experimentally probed that this attack is not promoted by hydroxyl radicals, as reported elsewhere [27].

From the PCXEs, three different reaction paths (RP) can be taken place:

RP1: The sulfate anion radical promoted the abstraction of a hydrogen atom from the PCXEs ring producing the releasing of Cl^- (RP1 in Fig. 8) forming tetrachlorocyclohexene (TCXEs). This reaction continues until the trichlorobenzene (TCBs) isomers are formed, releasing 3 mol of Cl^- per mol of Lindane. The sulfate anion radical can easily oxidate and dechlorinate TCB isomers. The radical sulfate can oxidize the aromatic ring of TCB isomers to a chlorinated phenolic compound (Cl-PhOs) [15,37,38]. Different TCB and Cl-PhOs isomers in this reaction can produce since the ring has different positions for radical

sulfate attack. The latter can be influenced by both steric hindrance and resonance stability [15,39]. However, small amounts of chlorinated cyclic organic compounds were detected by GC/ECD, as shown in Table 3. In addition, the formation of ring opening and cleavage by-products are also expected [37]. These intermediate byproducts can mineralize into CO_2 , H_2O and Cl^- [15,40].

RP2: The sulfate radical can react with a hydrogen atom close to the double bond in the PCXE ring [15,41]. A chlorocyclohexanyl radical is produced, and it can react by two different paths named RP2a and RP2b in Fig. 8. In RP2a, the organic radical generates a double bond, releasing the chloride radical that reacts with the hydrogen atoms, dechlorinating PCXE to the TCB isomers. These compounds can generate chlorophenol isomers following the mechanism mentioned above.

RP3: In this route, the chlorocyclohexanyl radical can react with a sulfate radical to generate an organosulfate salt, in a mechanism similar to that proposed by Ren et al. [35], these byproducts could not be identified with the analytical methods used, but their presence could explain the low dechlorination degree detected in the early stages of the reaction.

The opening of the carbon ring can be expected in the RPs of Fig. 8, but the reaction is only shown in RP3 to illustrate the radical mechanism. The sulfate radical can develop the addition of the electrophilic $\text{SO}_4^{\bullet-}$ to PCXE formed a carbon centered radical [15,35]. This radical can yield the ring opening following by a retro-Diels Alder elimination [42]. The byproducts generated were not identified by the analytical methods used here, but this can be expected, as was previously reported elsewhere [42].

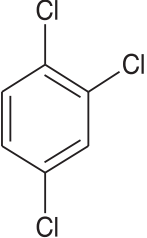
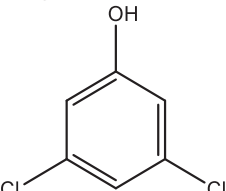
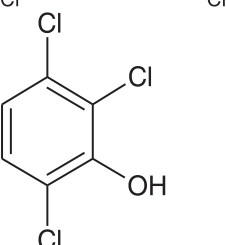
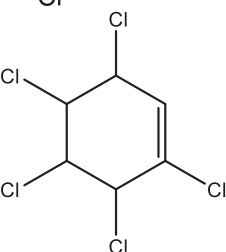
The chlorinated organic byproducts in Table 3 have also been identified but not quantified in other works in the literature studying the lindane elimination with AOPs [14,15] using UV light. In these works, the chloride mass balance using these byproducts was not accomplished.

4. Radical kinetic model

A kinetic model for lindane oxidation and chloride mineralization using persulfate and solar photoactivated ferrioxalate is developed. It is

Table 3

Chlorinated organic byproducts by GC/MS/SPME in run E5 (t = 60 min).

RT, min	formula	Name	C (mg/L)
3.83		1,2,4-trichlorobenzene (TCBs)	0.09
4.03		Phenol, n,m ^a -dichloro- (PhOs)	0.04
5.37		2,4,6-trichloro-phenol, (PhOs)	0.12
6.30/ 8.82 / 11.80 ^b		Pentachlorocyclohexene (PCXEs)	0.04 ^c

a: the isomers were not determined.

b: the isomers were quantified and identified in those retention times [1]

c: The concentration was determined as the sum of the three compounds.

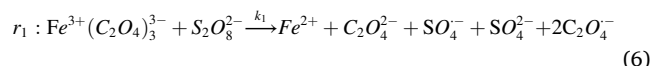
based on the action of sulfate radicals on lindane degradation. This model should explain the experimental evidence found, which can be summarized in the following assumptions:

- The positive effect of the photoactivation in the catalyst cycle.
- Unproductive reactions between the oxidant with oxalate or iron explain the small influence of increasing the concentration of these variables on the process efficiency.
- A lower dechlorination degree than lindane conversion obtained at early stages indicates the presence of organic chlorinated by-products.
- The small effect of lindane concentration on lindane conversion suggests a kinetic order close to the unity for the target pollutant

These findings can be modeled using a radical mechanism. This model includes the radical formation in the catalytic cycle, the unproductive reaction of the species (Fe^{2+} , Oxalate) with the generated radicals, the reaction of radicals with the target pollutant and the oxidation by-products and the effect of light in the catalyst cycle.

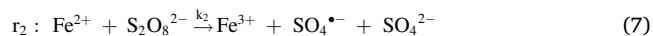
The model considers the following reactions:

- Dark reaction: The ferrioxalate complex react with PS to produce sulfate radicals in the absence of light



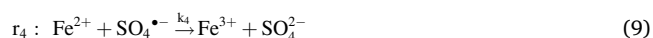
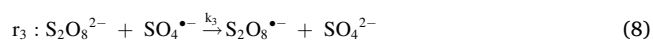
This reaction is similar to that considered by Kusic et al. [25] between Fe^{3+} complexed with organic aliphatic by-products and persulfate ($k_1 = 8.1 \cdot 10^{-4} \text{ mM}^{-1} \text{ min}^{-1}$). However, the value of k_1 using $\text{Fe}^{3+}(\text{C}_2\text{O}_4)_3^{3-}$ is not available in the literature.

- The Fe^{2+} produced reacts with PS to produce more sulfate radicals



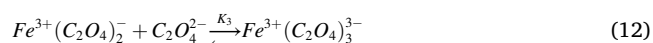
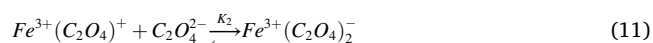
The value of k_2 is available in the literature with reported values $1 \text{ mM}^{-1} \text{ min}^{-1}$ [25] or $0.44 \text{ mM}^{-1} \text{ min}^{-1}$ [43]. In this work a value of $1 \text{ mM}^{-1} \text{ min}^{-1}$ have been considered.

- Sulfate radicals can react with pollutants (lindane and chlorinated organic byproducts) but also be consumed in non-productive reactions with persulfate and iron (II), as summarized following:

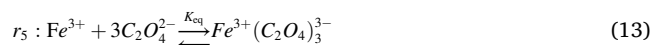


The value of k_3 is available in the literature with reported values of $3.97 \cdot 10^4 \text{ mM}^{-1} \text{ min}^{-1}$ [25]. The value of k_4 is available in the literature with reported values $1.30 \cdot 10^7 \text{ mM}^{-1} \text{ min}^{-1}$ [43] and $6 \cdot 10^7 \text{ mM}^{-1} \text{ min}^{-1}$ [44]. The value of this constant has been calculated in this work.

- The Fe^{3+} formed is in equilibrium with the free oxalate anion in the media



Being the global reaction between Fe^{3+} and $\text{C}_2\text{O}_4^{2-}$ to form the complex $\text{Fe}^{3+}(\text{C}_2\text{O}_4)_3^{3-}$ that summarized in Eq. (13) with $K_{\text{eq}} = 5 \cdot 10^{10} \text{ mM}^{-3}$ [45] from the database of MINQTEQ software [46].



- Sulfate radical can also react with free oxalate anion, as follows:



Value of $k_6 = 3.36 \cdot 10^5 \text{ mM}^{-1} \text{ min}^{-1}$ has been reported in the literature for the reaction of sulfate radical with organic aliphatic by-products [25], being this the value used in this work.

- Considering the mechanism proposed in Fig. 8, the reaction of sulfate radical with lindane will produce the first chlorinated by-products, named P₁



The value of k_7 between sulfate radicals and lindane has also been reported in the literature but within a wide range of values. He et al. [34] give a value of $k_7 = 5.37 \cdot 10^5 \text{ mM}^{-1} \text{ min}^{-1}$ while Khan et al. [15]

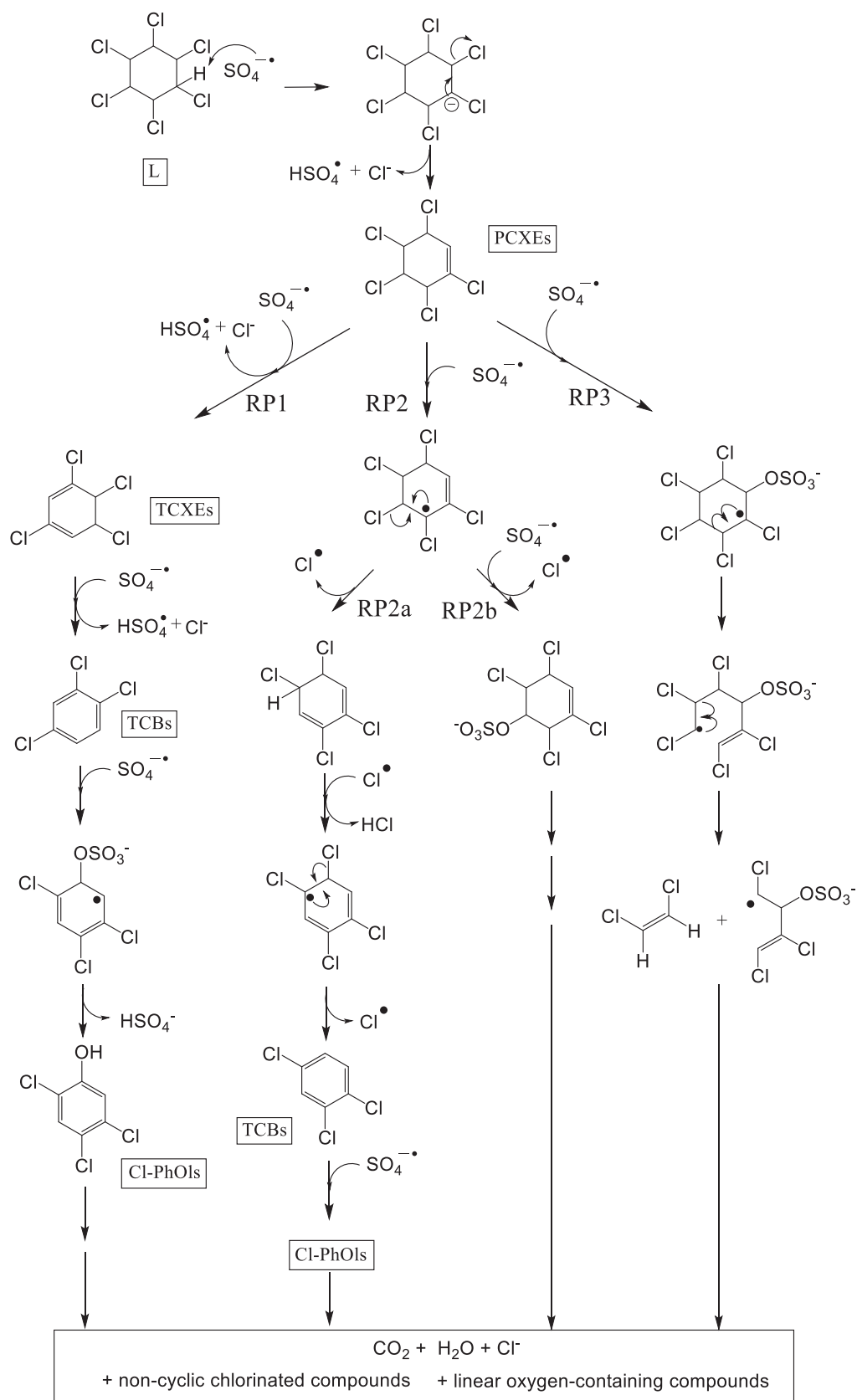


Fig. 8. Proposed reaction mechanism of $\text{SO}_4^{\bullet-}$ oxidation of Lindane. RP denoted the different reaction paths in the radical sulfate attack.

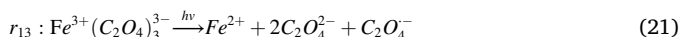
provide a value of $k_7 = 7.8 \cdot 10^7 \text{ mM}^{-1} \text{ min}^{-1}$, both works using competitive methods to obtain the kinetic constant k_7 . Therefore, this value will be estimated in this work from data fitting. The number of sulfate radicals involve in reaction 7 is named x .

- Taking into account the oxidation route proposed for lindane dechlorination (Fig. 8), the organic by-products produced can react with more sulfate radicals, with successive losses of chloride from the molecule, obtaining as final products oxygenated non-cyclic compounds or even CO_2 . The following reaction path has been proposed:



It has been assumed that all chlorinated byproducts (P_1 to P_5) react with the same number of sulfate radicals (x) and with the same kinetic constant k_8 . The number of chloride atoms decreases from 5 to 1 in P_1 to P_5 , with P_6 being a by-product completely dechlorinated. The value of k_8 must be estimated by data fitting

- The photodecomposition rate of the ferrioxalate with light has been considered, as shown in Eq. (21) [25]. This reaction enhances the reduction of Fe^{3+} to Fe^{2+} and Fe^{2+} activate PS to produce sulfate radicals (Eq. (9))



photosensitive agent. Units of $r(r_1 \text{ to } r_{13})$ are $\text{mM} \cdot \text{min}^{-1}$, related to the total volume of the batch system. Kinetic equations considered in the model are summarized in Eq. (23).

$$\begin{pmatrix} r_1 \\ r_2 \\ r_3 \\ r_4 \\ r_5 \\ r_6 \\ r_7 \\ r_8 \\ r_9 \\ r_{10} \\ r_{11} \\ r_{12} \\ r_{13} \end{pmatrix} = \begin{pmatrix} k_1 \cdot C_{\text{Fe}^{3+}} \cdot (\text{C}_2\text{O}_4)_3^{3-} \cdot C_{\text{PS}} \\ k_2 \cdot C_{\text{Fe}^{2+}} \cdot C_{\text{PS}} \\ k_3 \cdot C_{\text{PS}} \cdot C_{\text{SO}_4^-} \\ k_4 \cdot C_{\text{PS}} \cdot C_{\text{SO}_4^-} \\ k_5 \cdot \left(C_{\text{Fe}^{3+}} \cdot C_{\text{C}_2\text{O}_4^{2-}}^3 - C_{\text{Fe}^{2+}}(\text{C}_2\text{O}_4)_3^{3-} / k_{\text{eq}} \right) \\ k_6 \cdot C_{\text{C}_2\text{O}_4^{2-}} \cdot C_{\text{SO}_4^-} \\ k_7 \cdot C_{\gamma\text{-HCH}} \cdot C_{\text{SO}_4^-} \\ k_8 \cdot C_{P_1} \cdot C_{\text{SO}_4^-} \\ k_8 \cdot C_{P_2} \cdot C_{\text{SO}_4^-} \\ k_8 \cdot C_{P_3} \cdot C_{\text{SO}_4^-} \\ k_8 \cdot C_{P_4} \cdot C_{\text{SO}_4^-} \\ k_8 \cdot C_{P_5} \cdot C_{\text{SO}_4^-} \\ e^a(z, t)_{V_R} \Phi_G \cdot V_{\text{irr}} / V_t \end{pmatrix} \quad (23)$$

The mass balance for the j specie in a batch reactor (assuming perfect mixing) can be written by Eq. (24).

$$\frac{dC_j}{dt} = R_j = \sum_{i=1}^{NR=10} \nu_{ij} \cdot r_i \quad (24)$$

being R_j and C_j , the production rate ($\text{mM} \cdot \text{min}^{-1}$) and concentration (mM), respectively, of the j specie. ν_{ij} is the stoichiometric coefficient of the compound j in reaction i ($\nu_{ij} < 0$ for reactant and $\nu_{ij} > 0$ for products). The ν^T -matrix (species-reactions) is represented in Eq. (25).

$$\begin{pmatrix} R_{\text{PS}} \\ R_{\text{Fe}^{2+}} \\ R_{\text{C}_2\text{O}_4^{2-}} \\ R_{\gamma\text{-HCH}} \\ R_{P_1} \\ R_{P_2} \\ R_{P_3} \\ R_{P_4} \\ R_{P_5} \\ R_{\text{SO}_4^{\bullet-}} \end{pmatrix} = \begin{pmatrix} -1 & -1 & -1 & 0 & 0 & 0 & 0 & 0 & 0 & 0 & 0 & 0 & 0 \\ 1 & -1 & 0 & -1 & 0 & 0 & 0 & 0 & 0 & 0 & 0 & 0 & 1 \\ 1 & 0 & 0 & 0 & -3 & -1 & 0 & 0 & 0 & 0 & 0 & 0 & 2 \\ 0 & 0 & 0 & 0 & 0 & 0 & -1 & 0 & 0 & 0 & 0 & 0 & 0 \\ 0 & 0 & 0 & 0 & 0 & 0 & 1 & -1 & 0 & 0 & 0 & 0 & 0 \\ 0 & 0 & 0 & 0 & 0 & 0 & 0 & 1 & -1 & 0 & 0 & 0 & 0 \\ 0 & 0 & 0 & 0 & 0 & 0 & 0 & 0 & 1 & -1 & 0 & 0 & 0 \\ 0 & 0 & 0 & 0 & 0 & 0 & 0 & 0 & 0 & 1 & -1 & 0 & 0 \\ 0 & 0 & 0 & 0 & 0 & 0 & 0 & 0 & 0 & 0 & 1 & -1 & 0 \\ 1 & 1 & -1 & -1 & 0 & -1 & -1 & -x & -x & -x & -x & -x & 0 \end{pmatrix} \begin{pmatrix} r_1 \\ r_2 \\ r_3 \\ r_4 \\ r_5 \\ r_6 \\ r_7 \\ r_8 \\ r_9 \\ r_{10} \\ r_{11} \\ r_{12} \\ r_{13} \end{pmatrix}$$

The reaction rate of ferrioxalate photoactivation can be calculated by Eq. (22), considering the value of the local volumetric rate of photon absorption (LVRPA). The photon absorption rate is a function of the time and position in the reactor. Hence, it is necessary to calculate this rate at each point inside the reactor to obtain an average value over the irradiated volume [21,33].

$$r_{13} = \langle e^a(z, t) \rangle_{V_{\text{irr}}} \Phi_G \cdot V_{\text{irr}} / V_t \quad (22)$$

where $\langle e^a(z, t) \rangle_{V_R}$ is the average value of the LVRPA ($\text{EL}^{-1} \text{ min}^{-1}$) in the irradiated volume of the reactor V_{irr} (L), Φ_G is the global quantum yield in $\text{mmol} \cdot \text{E}^{-1}$ and V_t (L) is the total volume of the batch reactor (sum of liquid in the storage tank and the reactor). The quantum yield Φ_G of a photochemical reaction of a photosensitive agent is defined as the moles of photosensitive agent reacted per Einstein of light absorbed by the

With the initial condition:

$$C_j = C_{j,0} = 0 \quad (25)$$

The oxalate concentration experimentally measured ($C_{\text{ox-m}}$) corresponds to the sum of free oxalate anions and oxalate in the ferrioxalate complex:

$$C_{\text{ox-m}} = 3 \cdot C_{\text{Fe}^{3+}}(\text{C}_2\text{O}_4)_3^{3-} + C_{\text{C}_2\text{O}_4^{2-}} \quad (26)$$

The concentration of species containing iron ($C_{\text{Fe}^{3+}}(\text{C}_2\text{O}_4)_3^{3-}, \text{Fe}^{2+}, \text{Fe}^{3+}$) in the aqueous solution corresponds to the initial amount of Fe^{3+} added, before complexation (initial Fe^{2+} was zero):

$$C_{Fe^{3+}O} = C_{Fe^{3+}(C_2O_4)_3^{3-}} + C_{Fe^{2+}} + C_{Fe^{3+}} \quad (27)$$

Total chloride in the reaction media is calculated as:

$$C_{Cl^-} = 6C_{\gamma-HCHO} - 6C_{\gamma-HCH} - 5C_{P_1} - 4C_{P_2} - 3C_{P_3} - 2C_{P_4} - C_{P_5} \quad (28)$$

The differential equation system was integrated to obtain the concentration-time profiles of the different species involved in the reaction system. Experimental values of Lindane, chloride, total oxalate and persulfate conversion with time were fitted to the kinetic model above and the kinetic constant k_1 , k_4 , k_7 , k_8 and parameters x (in Eqs (15)–(20)) and Φ_G were calculated. Values of other kinetic constants in the model and equilibrium constant K_{eq} in Eq. (13) were taken from the literature. The following assumptions were considered:

- Equilibrium in Eq. (11) is reached instantaneously.

$$r_5 = 0 \quad (29)$$

- Pseudo-stationary state approach was applied to the concentration of sulfate radical:

$$\frac{dC_{SO_4^{\bullet-}}}{dt} = 0 \quad (30)$$

- To compute the average value of the LVRPA over the irradiated volume, $\langle e^a(z, t) \rangle_{V_R}$, it is necessary to know the local volumetric rate of photon absorption ($e^a(z, t, \lambda)$) at each reactor position (z), time (t) and wavelength (λ). A one-dimensional radiation field model has been used to calculate the $e^a(z, t, \lambda)$, being z the axial coordinate of the reactor (see Fig. 1) as described in Eq. (31) [47].

$$e^a(z, t, \lambda) = q_w(\lambda) \cdot \kappa_\lambda \cdot \exp(-\kappa_\lambda^T \cdot z) \quad (31)$$

being $q_w(\lambda)$ ($E \cdot \min^{-1} \cdot \text{cm}^{-2}$) the discretized spectral radiation flux incident at the reactor window for each wavelength. This value was measured experimentally (details are provided in Text SM2, and the $q_w(\lambda)$ values are given in Table SM1).

Parameters κ_λ and κ_λ^T are the volumetric absorption coefficient at each wavelength of the specie absorbing light and the volumetric absorption coefficient of the medium, respectively, both in cm^{-1} . Considering the high value of K_{eq} in (13), $Fe^{3+}(C_2O_4)_3^{3-}$, is the dominant ferrioxalate specie under the reaction conditions. Therefore, the only specie contributing to light absorption in the reaction media is this ferrioxalate complex ($\kappa_\lambda = \kappa_\lambda^T$). The molar absorptivity of ferrioxalate, α_λ ($\text{mM}^{-1} \cdot \text{cm}^{-1}$), is used to calculate the absorption coefficient, κ_λ , as a function of the molar concentration of the specie $Fe^{3+}(C_2O_4)_3^{3-}$, as indicated in Eq. (32).

$$\kappa_\lambda^T = \kappa_\lambda = \alpha_\lambda \cdot C_{Fe^{3+}(C_2O_4)_3^{3-}} \quad (32)$$

The wavelength range able to photoactivate the ferrioxalate complex is from $\lambda_{\min} = 300 \text{ nm}$ to $\lambda_{\max} = 550 \text{ nm}$ [21,48]. Values of α_λ for ferrioxalate complex were experimentally obtained as a function of the radiation wavelengths in the range studied. Details are provided in the SM as Text SM3, and the values for each wavelength are provided in Table SM1.

The average value of the LVRPA in the wavelength above cited, $e^a(z, t)$ at the axial reactor coordinate z , is calculated integrating $e^a(z, t, \lambda)$ (defined in Eq. (31)), as follows:

$$e^a(z, t) = \int_{\lambda_{\min}}^{\lambda_{\max}} e^a(z, t, \lambda) d\lambda \quad (33)$$

The volumetric average of the $e^a(z, t)$ in the irradiated reactor volume, $\langle e^a(x, t) \rangle_{V_{irr}}$, is calculated considering that $e^a(z, t)$ is the same at any cross-section point located at the axial coordinate z . Therefore, Eq. (33)

is integrated with the axial coordinate of the reactor, as shown in Eq. (34), being L_{irr} the length of the irradiated reactor (10 cm).

$$e^a(z, t)_{V_R} = \frac{1}{L_{irr}} \int_0^{L_{irr}} e^a(x, t) dz = \frac{1}{L_{irr}} \sum_{\lambda} q_w(\lambda) \cdot [1 - \exp(-\kappa_\lambda \cdot L_{irr})] \quad (34)$$

Solving the problem is composed of a set of differential and algebraic equations. It was implemented in ModelBuilder 7.1.0 provided in the gPROMS suit, and the algorithm DASOLV was used to simulate the reaction system. DASOLV is based on a variable time step, variable order, and Backward Differentiation Formulae (BDF) [49]. Experimental data of lindane conversion, dechlorination degree, oxidant conversion and total oxalate conversion were fitted to the model in Eqs. (23)–(34). The estimated parameters were calculated by minimizing the sum of quadratic squares (SQR), defined in Eq. (35), which is shown in Table 4, with the confidence interval (CI) (95%) of the parameters and the SQR for each variable and the SQRtotal.

$$SQR = \sum \left(\left(X_{j, \exp} - X_{j, \text{cal}} \right)^2 \right)_{j=L, PS, Cl^-, ox-m}, \quad (35)$$

The kinetic constant of lindane with hydroxyl radical found by Nioti et al. [14] was $8.34 \cdot 10^4 \text{ mM}^{-1} \cdot \text{min}^{-1}$. A higher kinetic constant of $1.21 \cdot 10^6 \text{ mM}^{-1} \cdot \text{min}^{-1}$ for the reaction between sulfate radicals and lindane has been obtained in this work. Both kinetic values confirm the higher reactivity of sulfate radicals against lindane compared to hydroxyl radicals, in agreement with the findings of Conte et al. [27]. The kinetic constant here obtained is in the range reported by He et al. [34] $k_7 = 5.37 \cdot 10^5 \text{ mM}^{-1} \cdot \text{min}^{-1}$ and Khan et al. [15] ($k_7 = 7.8 \cdot 10^7 \text{ mM}^{-1} \cdot \text{min}^{-1}$) for the reaction between lindane and sulfate radicals. Differences can be attributed to these works in the literature used competitive methods to obtain the kinetic constant k_7 . In addition, the estimated k_1 is close to those reported in the literature [25].

The global quantum yield Φ_G ($\text{mmol} \cdot \text{E}^{-1}$) obtained in this work is close to the values reported in the literature for organic aliphatic by-products complexed with Fe^{3+} [21,25].

Lindane, oxalate, persulfate, and chloride mineralization degree with time at the conditions of runs in Table 2 have been predicted with the model in Eqs. (23)–(34) and kinetic parameters in Table 4 (other kinetic constants in the model are obtained from the literature, as indicated before). A good agreement has been obtained between experimental (symbols) and simulated (lines) values despite the high number of kinetic parameters taken from the literature and the assumptions made.

The importance of unproductive reactions in Eqs. (9) and (3) explains the relatively low enhancement in lindane conversion and dechlorination degree obtained by increasing the iron or persulfate concentration, respectively.

4.1. Kinetic model validation

The kinetic model proposed has been validated with a new experiment (V1) carried out using an iron concentration out of the range considered in Table 2 (0.020 concentration). PS, Oxalate, lindane concentration, temperature and radiation have been fixed at 3.25 mM, 0.20 mM, 0.021 mM, 25°C and $0.87 \cdot 10^{-7} \text{ Ecm}^{-2} \cdot \text{s}^{-1}$, respectively. Experimental values and simulated ones using the kinetic model in Eqs.

Table 4

Estimated parameters and confidence interval (CI) (95%) of the parameters calculated for the kinetic model in Eqs. (6)–(22).

PARAMETER	Value	SQR	Value
$k_1 (\text{mM}^{-1} \cdot \text{min}^{-1})$	$3.28 \cdot 10^{-4} \pm 1.66 \cdot 10^{-6}$	X_L	0.36
$k_4 (\text{mM}^{-1} \cdot \text{min}^{-1})$	$1.04 \cdot 10^8 \pm 4.12 \cdot 10^5$	X_{Ox-m}	0.67
$k_7 (\text{mM}^{-1} \cdot \text{min}^{-1})$	$1.21 \cdot 10^6 \pm 8.61 \cdot 10^4$	X_{Cl^-}	1.10
$k_8 (\text{mM}^{-1} \cdot \text{min}^{-1})$	$6.98 \cdot 10^6 \pm 1.20 \cdot 10^6$	X_{PS}	0.46
x	1.2 ± 0.25	TOTAL	2.59
$\Phi_G \text{ mmol E}^{-1}$	918 ± 14		

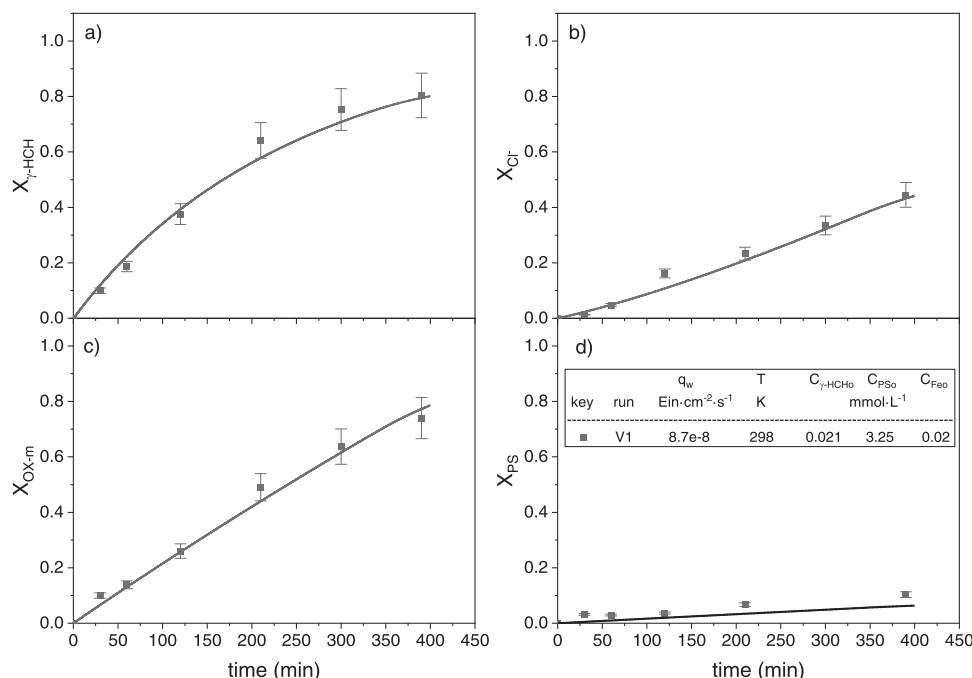


Fig. 9. Validation of predicted value of lindane conversion (a), dechlorination degree (b), oxalate conversion (c) and oxidant conversion (d) in the validation run V1. Symbols depicted experimental values. Lines show predicted values with Eqs. (23)–(34).

(23)–(34) to are shown in Fig. 9. The good agreement between experimental and simulated values validates the kinetic model proposed.

5. Conclusions

Oxidation and dechlorination of lindane (up to 9.3 mg L⁻¹) in the aqueous phase were successfully achieved with the oxidation system proposed here. The ferrioxalate complex was photoactivated by solar light, reducing the Fe³⁺ to Fe²⁺, increasing the generation of sulfate radicals by reacting the formed ferrous species with the oxidant. The positive effect of the light in the catalyst cycle has been confirmed, being this enhancement more significant on the lindane dechlorination. Unproductive reactions between oxalate, Fe²⁺ or PS with the sulfate radicals must be considered to explain the disappearance of the catalyst and the relatively small effect noticed in lindane conversion and dechlorination when increasing the oxidant or catalyst concentration. The catalyst, oxidant concentration, and the circumneutral pH used here are below the limits of these parameters in discharges. Moreover, the solar light avoids the use of UV lamps that require high energy cost. Dechlorination degree was lower than lindane conversion at early stages, suggesting the presence of organic chlorinated by-products. Chlorinated byproducts identified by the analytical methods do not allow the chloride mass balance close appropriately at the early stages of lindane oxidation. A reaction path also considering the formation of organosulfur salts has been proposed.

The results here encourage using solar light, persulfate and ferrioxalate complex to remediate aqueous phases contaminated by chlorinated pesticides. Experiments using other chlorinated organic compounds, such as HCHs mixtures, complex natural groundwater matrixes with organic and inorganic substances, and not simulated but direct solar light, will be carried out in future works to implement this technology on the field scale.

CRediT authorship contribution statement

Leandro O. Conte: Investigation, Methodology. **Giuseppe Legnettino:** Investigation, Methodology. **David Lorenzo:** Data curation, Formal analysis, Software, Validation, Writing – review & editing.

Salvador Cotillas: Data curation, Formal analysis, Methodology, Writing – review & editing. **Marina Prisciandaro:** Supervision, Writing – review & editing. **Aurora Santos:** Conceptualization, Funding acquisition, Project administration, Resources, Supervision, Validation, Visualization, Writing – original draft, Writing – review & editing.

Declaration of Competing Interest

The authors declare that they have no known competing financial interests or personal relationships that could have appeared to influence the work reported in this paper.

Data availability

No data was used for the research described in the article.

Acknowledgments

This research is part of the project PID2019–105934RB-I00 funded by MCIN/AEI/10.13039/501100011033 and project S2018/EMT-4317 (CARESOIL CM) funded by the Community of Madrid. Leandro O. Conte gratefully acknowledges the European Union's Horizon 2020 research and innovation Programme for the Marie Skłodowska-Curie Grant Agreement no. 844209.

Appendix A. Supporting information

Supplementary data associated with this article can be found in the online version at [doi:10.1016/j.apcatb.2022.122288](https://doi.org/10.1016/j.apcatb.2022.122288).

References

- [1] A. Santos, J. Fernandez, J. Guadano, D. Lorenzo, A. Romero, Chlorinated organic compounds in liquid wastes (DNAPL) from lindane production dumped in landfills in Sabinanigo (Spain), *Environ. Pollut.* 242 (2018) 1616–1624, <https://doi.org/10.1016/j.envpol.2018.07.117>.
- [2] D. Romano, M. Vega, E. Uotila, ERA-Consult Madrid, European Parliament, Directorate-General for Internal Policies, Policy Department C: Citizens' Rights, Constitutional Affairs, Lindane (persistent Organic Pollutant) in the EU: Study, European Parliament, 2016.

- [3] J. Vijgen, B. Fokke, G. van de Coterlet, K. Amstaetter, J. Sancho, C. Bensaïah, R. Weber, European cooperation to tackle the legacies of hexachlorocyclohexane (HCH) and lindane, *Emerg. Contam.* 8 (2022) 97–112, <https://doi.org/10.1016/j.emcon.2022.01.003>.
- [4] B. Biosca, L. Arévalo-Lomas, M. Izquierdo-Díaz, J. Díaz-Curiel, Detection of chlorinated contaminants coming from the manufacture of lindane in a surface detritic aquifer by electrical resistivity tomography, *J. Appl. Geophys.* 191 (2021), <https://doi.org/10.1016/j.jappgeo.2021.104358>.
- [5] J. Fernandez, M.A. Arjol, C. Cacho, POP-contaminated sites from HCH production in Sabinanigo, Spain, *Environ. Sci. Pollut. Res.* 20 (2013) 1937–1950, <https://doi.org/10.1007/s11356-012-1433-8>.
- [6] B. Lodha, P. Bhat, M.S. Kumar, A.N. Vaidya, S. Mudliar, D.J. Killedar, T. Chakrabarti, Bioisomerization kinetics of γ -HCH and biokinetics of *Pseudomonas aeruginosa* degrading technical HCH, *Biochem. Eng. J.* 35 (2007) 12–19, <https://doi.org/10.1016/j.bej.2006.12.015>.
- [7] M. Kumari, P. Ghosh, Swati, I.S. Thakur, Development of artificial consortia of microalgae and bacteria for efficient biodegradation and detoxification of lindane, *Bioresour. Tech. Rep.* 10 (2020), 100415, <https://doi.org/10.1016/j.biteb.2020.100415>.
- [8] J.A. Salam, N. Das, Degradation of lindane by a novel embedded bio-nano hybrid system in aqueous environment, *Appl. Microbiol. Biotechnol.* 99 (2015) 2351–2360, <https://doi.org/10.1007/s00253-014-6112-x>.
- [9] B.C. Okeke, T. Siddique, M.C. Arbustain, W.T. Frankenberger, Biodegradation of γ -Hexachlorocyclohexane (Lindane) and α -Hexachlorocyclohexane in Water and a Soil Slurry by a *Pandora* Species, *J. Agric. Food Chem.* 50 (2002) 2548–2555, <https://doi.org/10.1021/jf011422a>.
- [10] D. Kumar, R. Pannu, Perspectives of lindane (γ -hexachlorocyclohexane) biodegradation from the environment: a review, *Bioresour. Bioprocess.* 5 (2018) 29, <https://doi.org/10.1186/s40643-018-0213-9>.
- [11] A. Tor, M.E. Aydin, S. Aydin, M. Tabakci, F. Beduk, Removal of lindane from an aqueous solution by using aminopropyl silica gel-immobilized calix[6]arene, *J. Hazard. Mater.* 262 (2013) 656–663, <https://doi.org/10.1016/j.jhazmat.2013.09.026>.
- [12] I.D. Patil, Y.S. Patil, B.L. Pangarkar, Removal of lindane from wastewater using liquid-liquid extraction process, *Pol. J. Chem. Technol.* 15 (2013) 81–84, <https://doi.org/10.2478/pjct-2013-0050>.
- [13] M.A. Oturan, J.J. Aaron, Advanced oxidation processes in water/wastewater treatment: Principles and applications. A review, *Crit. Rev. Environ. Sci. Technol.* 44 (2014) 2577–2641, <https://doi.org/10.1080/10643389.2013.829765>.
- [14] I. Nitoi, T. Onicescu, P. Oancea, Mechanism and kinetic study for the degradation of lindane by photo-Fenton process, *J. Ind. Eng. Chem.* 19 (2013) 305–309, <https://doi.org/10.1016/j.jiec.2012.08.016>.
- [15] S. Khan, X. He, J.A. Khan, H.M. Khan, D.L. Boccelli, D.D. Dionysiou, Kinetics and mechanism of sulfate radical- and hydroxyl radical-induced degradation of highly chlorinated pesticide lindane in UV/peroxymonosulfate system, *Chem. Eng. J.* 318 (2017) 135–142, <https://doi.org/10.1016/j.cej.2016.05.150>.
- [16] C.M. Domínguez, N. Oturan, A. Romero, A. Santos, M.A. Oturan, Optimization of electro-Fenton process for effective degradation of organochlorine pesticide lindane, *Catal. Today* 313 (2018) 196–202, <https://doi.org/10.1016/j.cattod.2017.10.028>.
- [17] M. Ansari, M. Sharifian, M. Farzadkia, Removal of lindane in water by non-thermal plasma: Parametric optimization, kinetic study, energy yield evaluation, and toxicity assessment, *Sep. Purif. Technol.* 299 (2022), 121549, <https://doi.org/10.1016/j.seppur.2022.121549>.
- [18] C.M. Domínguez, N. Oturan, A. Romero, A. Santos, M.A. Oturan, Removal of organochlorine pesticides from lindane production wastes by electrochemical oxidation, *Environ. Sci. Pollut. Res.* 25 (2018) 34985–34994, <https://doi.org/10.1007/s11356-018-1425-4>.
- [19] S. Khan, C. Han, M. Sayed, M. Sohail, S. Jan, S. Sultana, H.M. Khan, D. D. Dionysiou, Exhaustive photocatalytic lindane degradation by combined simulated solar light-activated nanocrystalline TiO₂ and inorganic oxidants, *Catalysts* 9 (2019), <https://doi.org/10.3390/catal9050425>.
- [20] S. Khan, M. Sohail, C. Han, J.A. Khan, H.M. Khan, D.D. Dionysiou, Degradation of highly chlorinated pesticide, lindane, in water using UV/persulfate: kinetics and mechanism, toxicity evaluation, and synergism by H₂O₂, *J. Hazard. Mater.* 402 (2021), 123558, <https://doi.org/10.1016/j.jhazmat.2020.123558>.
- [21] L.O. Conte, A.V. Schenone, O.M. Alfano, Photo-Fenton degradation of the herbicide 2,4-D in aqueous medium at pH conditions close to neutrality, *J. Environ. Manag.* 170 (2016) 60–69, <https://doi.org/10.1016/j.jenvman.2016.01.002>.
- [22] M. Gholami Shirkoobi, R.D. Tyagi, P.A. Vanrolleghem, P. Drogui, Modelling and optimization of psychoactive pharmaceutical caffeine removal by electrochemical oxidation process: A comparative study between response surface methodology (RSM) and adaptive neuro fuzzy inference system (ANFIS), *Sep. Purif. Technol.* 290 (2022), <https://doi.org/10.1016/j.seppur.2022.120902>.
- [23] A.D. Ortiz-Marin, E.R. Bandala, K. Ramírez, G. Moeller-Chávez, L. Pérez-Estrada, B. Ramírez-Pereda, L.E. Amabilis-Sosa, Kinetic modeling of UV/H₂O₂, UV/sodium percarbonate, and UV/potassium peroxymonosulfate processes for albendazole degradation, *React. Kinet. Mech. Catal.* 135 (2022) 639–654, <https://doi.org/10.1007/s11444-021-02152-z>.
- [24] E. Gualda-Alonso, P. Soriano-Molina, J.L. García Sánchez, J.L. Casas López, J.A.S.á nchez Pérez, Mechanistic modeling of solar photo-Fenton with Fe³⁺-NTA for microcontaminant removal, *Appl. Catal. B Environ.* 318 (2022), <https://doi.org/10.1016/j.apcatb.2022.121795>.
- [25] H. Kusic, I. Peternel, S. Ukic, N. Koprivanac, T. Bolanca, S. Papic, A.L. Bozic, Modeling of iron activated persulfate oxidation treating reactive azo dye in water matrix, *Chem. Eng. J.* 172 (2011) 109–121, <https://doi.org/10.1016/j.cej.2011.05.076>.
- [26] R. Zhang, Y. Yang, C.H. Huang, L. Zhao, P. Sun, Kinetics and modeling of sulfonamide antibiotic degradation in wastewater and human urine by UV/H₂O₂ and UV/PDS, *Water Res.* 103 (2016) 283–292, <https://doi.org/10.1016/j.watres.2016.07.037>.
- [27] L.O. Conte, S. Cotillas, A. Sánchez-Yepes, D. Lorenzo, A. Santos, LED visible light assisted photochemical oxidation of HCHs in aqueous phases polluted with DNAPL, *Process Saf. Environ. Prot.* 168 (2022) 434–442, <https://doi.org/10.1016/j.psep.2022.10.015>.
- [28] S.L. Murov, I. Carmichael, G.L. Hug, *Handbook of Photochemistry*, CRC Press, 1993.
- [29] D. Lorenzo, R. García-Cervilla, A. Romero, A. Santos, Partitioning of chlorinated organic compounds from dense non-aqueous phase liquids and contaminated soils from lindane production wastes to the aqueous phase, *Chemosphere* 239 (2020), 124798, <https://doi.org/10.1016/j.chemosphere.2019.124798>.
- [30] A. Santos, C.M. Domínguez, D. Lorenzo, R. García-Cervilla, M.A. Lominchar, J. Fernandez, J. Gomez, J. Guadano, Soil flushing pilot test in a landfill polluted with liquid organic wastes from lindane production, *Heliyon* 5 (2019), e02875, <https://doi.org/10.1016/j.heliyon.2019.e02875>.
- [31] R. García-Cervilla, A. Santos, A. Romero, D. Lorenzo, Partition of a mixture of chlorinated organic compounds in real contaminated soils between soil and aqueous phase using surfactants: Influence of pH and surfactant type, *J. Environ. Chem. Eng.* 9 (2021), <https://doi.org/10.1016/j.jece.2021.105908>.
- [32] C. Liang, C.-F. Huang, N. Mohanty, R.M. Kurakalva, A rapid spectrophotometric determination of persulfate anion in ISCO, *Chemosphere* 73 (2008) 1540–1543, <https://doi.org/10.1016/j.chemosphere.2008.08.043>.
- [33] L.O. Conte, A.V. Schenone, O.M. Alfano, Ferrioxalate-assisted solar photo-Fenton degradation of a herbicide at pH conditions close to neutrality, *Environ. Sci. Pollut. Res.* 24 (2017) 6205–6212, <https://doi.org/10.1007/s11356-016-6400-3>.
- [34] L. He, L. Bu, R. Spinney, D.D. Dionysiou, R. Xiao, Reactivity and reaction mechanisms of sulfate radicals with lindane: An experimental and theoretical study, *Environ. Res.* 201 (2021), 111523, <https://doi.org/10.1016/j.envres.2021.111523>.
- [35] H. Ren, J.A. Sedlak, M.J. Elrod, General mechanism for sulfate radical addition to olefinic volatile organic compounds in secondary organic aerosol, *Environ. Sci. Technol.* 55 (2021) 1456–1465, <https://doi.org/10.1021/acs.est.0c05256>.
- [36] X. Pan, J. Wei, M. Zou, J. Chen, R. Qu, Z. Wang, Products distribution and contribution of (de)chlorination, hydroxylation and coupling reactions to 2,4-dichlorophenol removal in seven oxidation systems, *Water Res.* 194 (2021), 116916, <https://doi.org/10.1016/j.watres.2021.116916>.
- [37] G.P. Anipsitakis, D.D. Dionysiou, M.A. Gonzalez, Cobalt-mediated activation of peroxymonosulfate and sulfate radical attack on phenolic compounds. implications of chloride ions, *Environ. Sci. Technol.* 40 (2006) 1000–1007, <https://doi.org/10.1021/es050634b>.
- [38] P. Neta, V. Madhavan, H. Zemel, R.W. Fessenden, Rate constants and mechanism of reaction of sulfate radical anion with aromatic compounds, *J. Am. Chem. Soc.* 99 (1977) 163–164, <https://doi.org/10.1021/ja00443a030>.
- [39] M.G. Antoniou, J.A. Shoemaker, A. Adl Cruz, D.D. Dionysiou, Unveiling new degradation intermediates/pathways from the photocatalytic degradation of microcystin-LR, *Environ. Sci. Technol.* 42 (2008) 8877–8883, <https://doi.org/10.1021/es801637z>.
- [40] Y.R. Wang, W. Chu, Photo-assisted degradation of 2,4,5-trichlorophenol by Electro-Fe(II)/Oxone® process using a sacrificial iron anode: Performance optimization and reaction mechanism, *Chem. Eng. J.* 215–216 (2013) 643–650, <https://doi.org/10.1016/j.cej.2012.11.042>.
- [41] L.O. Conte, P. Querini, E.D. Albizzati, O.M. Alfano, Photonic and quantum efficiencies for the homogeneous photo-Fenton degradation of herbicide 2,4-D using different iron complexes, *J. Chem. Technol. Biotechnol.* 89 (2014) 1967–1974, <https://doi.org/10.1002/jctb.4284>.
- [42] R.W. Chadwick, J.J. Freal, G.W. Sovocool, C.C. Bryden, M.F. Copeland, The identification of three previously unreported lindane metabolites from mammals, *Chemosphere* 7 (1978) 633–640, [https://doi.org/10.1016/0045-6535\(78\)90085-1](https://doi.org/10.1016/0045-6535(78)90085-1).
- [43] S. Rodriguez, A. Santos, A. Romero, Oxidation of priority and emerging pollutants with persulfate activated by iron: Effect of iron valence and particle size, *Chem. Eng. J.* 318 (2017) 197–205, <https://doi.org/10.1016/j.cej.2016.06.057>.
- [44] P. Neta, R.E. Huie, A.B. Ross, Rate constants for reactions of inorganic radicals in aqueous solution, *J. Phys. Chem. Ref. Data* 17 (1988) 1027–1284.
- [45] R.M. Smith, A.E. Martell, R.J. Motekaitis, NIST critically selected stability constants of metal complexes database. NIST standard reference database 46, version 7.0. NIST, Gaithersburg, MD, USA, 2003.
- [46] J.P. Grustafsson, MINQT, ver 3.1, KTH SEED Stockholm, Sweden, 2020.
- [47] O.M. Alfano, R.L. Romero, A.E. Casano, A cylindrical photoreactor irradiated from the bottom-I. Radiation flux density generated by a tubular source and a parabolic reflector, *Chem. Eng. Sci.* 40 (1985) 2119–2127, [https://doi.org/10.1016/0009-2509\(85\)87030-5](https://doi.org/10.1016/0009-2509(85)87030-5).
- [48] H.J. Kuhn, S.E. Braslavsky, R. Schmidt, Chemical actinometry (IUPAC Technical Report), *Pure Appl. Chem.* 76 (2004) 2105–2146, <https://doi.org/10.1351/pac200476122105>.
- [49] Siemens, Process Systems Enterprise, gPROMS, 2022.